Journal of Solid Mechanics Vol. 12, No. 1 (2020) pp. 234-248
DOI: 10.22034/jsm.2019.1870627.1455

A New Numerical Study Method of Thermal Stress Distribution and Tortuosity Effectiveness in an Anode Porous Electrode for a Planar Solid Oxide Fuel Cell

I.E. Fahs *, M. Ghasemi

Mechanical Engineering Faculty, K. N. Toosi University of Technology, Tehran, Iran

Received 7 January 2020; accepted 10 March 2020

ABSTRACT

A fuel cell is an electro-chemical tool capable of converting chemical energy into electricity. High operating temperature of solid oxide fuel cell, between 700°C to 1000°C, causes thermal stress. Thermal stress causes gas escape, structure variability and cease operation of the SOFC before its lifetime. The purpose of the current paper is to present a method that predicts the thermal stress distribution in an anisotropic porous anode of planar SOFC. The coupled governing non-linear differential equations, heat transfer, fluid flow, mass transfer, mass continuity, and momentum are solved numerically. A code based on computational fluid dynamics (CFD), computational structural mechanics and finite element method (FEM) is developed and utilized. The code uses the generated data inside the porous anode in order to detect the temperature and the stress distribution using the Darcy's law and the Navier-Stokes equations. The numerical results used to govern the areas of high values of stresses were higher than the yield strength of materials. The results show that a highest thermal stress occurs at lower corners of the anode. The concentrated temperature occurs at the middle of the electrolyte-anode whereas the maximum pressure occurs at the middle of the upper and lower section of the anode.

Keywords: Solid oxide fuel cell (SOFC); Computational fluid dynamic; Finite elements method; Thermal stress; Anode.

1 INTRODUCTION

ONE of the greatest promising new energy technologies for high-energy efficiency are fuel cells, which are also environmental responsive and show fuel variety [1]. Fuel cells are electrochemical mechanism that transform the chemical energy into electrical and thermal energy. Solid oxide fuel cells (SOFCs), one of the different types of fuel cells, have gained attention due to their performance and fuel elasticity [2, 3]. In addition to that, they function in the high temperature variety, 700 °*C*–1000 °*C*. However, this technology still faces many challenges such as cost reduction and an extended lifetime operation. These challenges require prediction and prevention of internal thermal

*Corresponding author.
E-mail address: imadfahs@email.kntu.ac.ir (I.E.Fahs).

stresses. The SOFC technology still aspects many challenges such as reduce costs and an extended lifetime operation, which requires prediction and therefore prevention of internal thermal stresses. The thermal stress has recently concerned increasing attentions in the SOFC investigation community since it could, due to the formation of cracks, affect the lifetime of the cell. In order to inspect the influence of the functional parameters on the thermal stress performance of SOFCs, experimental techniques are used but these techniques take more time and more expenditure compared to simulation work. The latter has gained more attention due to its simplicity and as well as low cost compared to experimental conduction. The number of SOFC experimental and numerical research papers has shown a prosperous increase throughout the last 20 years [4-10]. Experimental studies typically emphasis on the estimation of materials and fuels, however, numerical ones focus on simulating the coupled chemical, physical and electrochemical incidence occurring in the cell (Pasaogullari and Wang) [11]. Several researchers had used three-dimensional to model the entire cell [12, 13]. The common objective of their research was to study the configuration and operating conditions on the general performance of the cell. On the other hand, other researchers tend to use two-dimensional (2D) models for tubular SOFCs because of their axial [14 -16]. Another class of studies analyses the phenomena that occur locally in the porous electrodes and in the electrolyte (Suwan Warangkul et al.) [17]. Recently, most researchers focus on the thermal stress inside the SOFC [18 - 20]. Celik et al. [18] studied the two dimensional stress and the thermal analysis in the anode-electrolyte boundary of a SOFC. They calculated the stresses produced within the different layers of the cell in order to estimate the degradation and delamination of (SOFCs) electrode-electrolyte, but their model does not cover coupling between heat, mass transfer and fluid flow. Luo et al. [19] studied the influence of anode porosity on thermal stress and decline probability of planar SOFC with attached compliant seal by finite element method. They showed discontinuous stresses along the plate thickness, which was due to the mismatching of material characteristic. Ho and Kosinski [20] studied the effect of heat source on the performance of a planar solid oxide fuel cell. They studied the effects of heat source location on the cell execution.

However, the purpose of the current paper is to present a method that illustrate the distribution of thermal stress in an anisotropic porous anode electrode in a planar SOFC. The main goal is to understand the effect of thermal stress and high temperature and its location for future remedy.

2 PROBLEM DEFINITION

The Diagram of the problem is represented in Fig.1. As shown in Fig. 1 the cell is consisting of 5 layers, anode, cathode, electrolyte, air channel and fuel channel. Tables 1 and 2 show the material properties and the geometrical parameters of the current study, respectively.

Table 1
Material properties of anode electrode.

	Anode
Material	Ni-YSZ
Density (kg/m^3)	6870
Young's modulus (GPa)	57
Poisson's Coefficient	0.28
Tensile yield strength (MPa)	115
Compressive strength (MPa)	100
Specific surface area (m^{-1})	1×10^{9}
Thermal expansion coefficient (K^{-1})	12.2×10^{-7}
Permeability (m^2)	1×10^{-12}
Electronic conductivity effectivity (S/m)	13195
Ionic conductivity effectivity(S/m)	0.51364
Stress intensity factor ($MPa.m^{0.5}$)	1.6

Table 2
Geometrical parameters of the anode electrode.

Channel length (mm)	60
Channel thickness (mm)	0.35
Anode thickness (mm)	0.06
Anode length (mm)	60

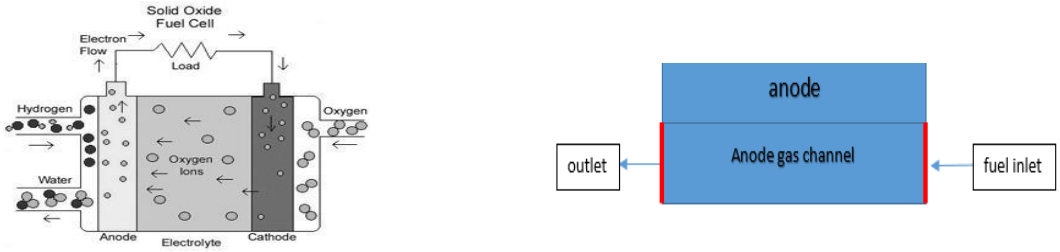

(a) (b)

Fig.1
(a) SOFC [20]. (b) Representation of anode electrode and anode gas channel.

All fluid properties vary with temperature and the fluid here is presumed to perform as an ideal gas. In addition to that, the flow is steady, compressible, two-dimensional and laminar. The electrolyte is fully impermeable and the electrodes are eclectic which intend the following reactions take place in the electrodes:

Anode reaction:

$$H_2 + O^{-2} \rightarrow H_2O + 2e^- \tag{1}$$

Cathode reaction:

$$\frac{1}{2}\, O_2 + 2e^- \rightarrow O^{-2} \tag{2}$$

The overall reaction is given by:

$$H_2 + \frac{1}{2}\, O_2 \rightarrow H_2O \tag{3}$$

2.1 Mass and momentum conservation

The continuity equation in anode porous electrode is given by [21]:

$$\nabla.(\rho \mathbf{u}) = \sum_j R_j \tag{4}$$

In which ρ is density and $\boldsymbol{u}$ is velocity vector. Mass depletion or creation occur due to electrochemical reactions which is represented in the right hand side of Eq. (4). Since electrochemical reactions occur in the catalyst layers, the mass source term is zero for other layers. R, the consumption rate for hydrogen (R_{H2}), water (R_{H2O}), are as follows, respectively:

$$R_{H_2} = \frac{-M_{H_2}}{2F} \times j_{loc,a} \tag{5}$$

$$R_{H_2O} = \frac{M_{H_2O}}{2F} \times j_{loc,a} \tag{6}$$

2.2 Momentum equation

The momentum equation for stationary and incompressible flow in porous anode electrodes with no body force is express by Darcy law as [25]:

$$\rho\mathbf{u}.\nabla\mathbf{u} = \nabla.\left(-p\mathbf{I} + \frac{\mu}{\in}\left(\nabla\mathbf{u} + (\nabla\mathbf{u})^T\right) - \frac{2\mu}{3}(\nabla.\mathbf{u})\mathbf{I}\right) + \rho\mathbf{g} - \left(\frac{\mu}{\kappa}\right)\mathbf{u} \tag{7}$$

where u is the flow velocity, κ is the permeability, μ is the dynamic viscosity, and P is absolute pressure. The momentum transport in fuel channel is applied by the Navier- Stokes equation.

$$\rho(\mathbf{u}.\nabla)\mathbf{u} = \nabla.\left[-p\mathbf{I} + \mu\left(\nabla\mathbf{u} + (\nabla\mathbf{u})^T\right)\right] + F \tag{8}$$

2.3 Species conservation

The species conservation equation id given by [22]:

$$\nabla.j_i + \rho(u.\nabla)\omega_i = R_i \tag{9}$$

j_i is the diffusive flux of the *ith* species, the mass fraction of *ith* species is ω_i, R_i is the rate of production of species. The relative mass flux vector can be written, using the Maxwell–Stefan equations for multi-component systems, as [16]:

$$j_i = -\rho w_i \sum_k D_{ik} d_k \tag{10}$$

d_k is the generalized driving force and D_{ik} is the Fick's law diffusion coefficient of species (multi-component), in which it can be determined by [22]:

$$D_{ik} = 1.883\times10^{-2} T^{1.5} \frac{\left(\frac{1}{M_i} + \frac{1}{M_k}\right)^{1/2}}{p\sigma_{ik}^2 \Omega_D} \tag{11}$$

where diffusion collision integral is Ω_D, characteristic length is σ and, M is the molecular weight. To study the mass transfer resistance in the porous electrodes, the multi-component Fick's diffusivities are corrected by the following equation:

$$D_{ik}^{eff} = \left(\frac{\varepsilon}{\tau}\right) D_{ik} \tag{12}$$

τ is the porous media tortuosity. The Dusty Gas Model (DGM) is applied to account for Knudsen diffusion in small pores. The effective DGM diffusion of coefficient ($D_{DGM,ik}^{eff}$) is defined as:

$$D_{DGM,ik}^{eff} = \frac{\left(\frac{\varepsilon}{\tau}\right)\left(D_{ik}, D_{KN,ik}\right)}{\left(D_{ik}, D_{KN,ik}\right)} \tag{13}$$

The Knudsen diffusivities coefficient $D_{KN,ik}$ and is calculated by kinetic theory of gases as follow:

$$D_{KN,ik}^{eff} = \frac{4}{3re\sqrt{\frac{R_u T\left(M_i + M_k\right)}{\pi M_i . M_k}}} \tag{14}$$

Effective pore radius is *re*, and R_u being the ideal gas constant.

2.4 Energy conservation

The porous electrode energy equation is given by:

The energy equation for laminar, steady, incompressible and low speed is given by [24]:

$$\nabla.\left(\rho C_p u T - K\nabla T\right) = Q \tag{15}$$

where ρ is density, C_p is heat capacity at constant pressure and Q is the heat source due to ion electronic transport resistance in each of the three layers and is determined by:

$$Q = \frac{j_{io}^2}{\sigma_{io}} \tag{16}$$

j_{io} and σ_{io} are the ionic current density and conductivity, respectively [25].

2.5 Charge conservation

Using Ohm's law, the governing electron conservation and ion transfer equations are as follows, respectively [26]:

$$\nabla.\left(-\sigma_e \nabla\varphi_e\right) = j_e \tag{17}$$

$$\nabla.\left(-\sigma_i \nabla\varphi_i\right) = j_i \tag{18}$$

where j_e and j_i are the electronic and ionic source, σ_e is electronic conductivity and σ_i is the ionic conductivity. The electrical and ionic charge source (j_e) and (j_i) for anode electrode are expressed by the Bulter–Volmer equation, respectively [27]:

$$j_{i,a} = -j_{e,a} = A_a j_{0,ref}^{H_2}\left(\frac{CH_2}{CH_{2,ref}}\right)^{\gamma H_2}\left[\exp\left(\frac{\alpha_a^a Fr)_{act,a}}{R_u T}\right) - \exp\left(-\frac{\alpha_c^a Fr)_{act,a}}{R_u T}\right)\right]\gamma H_2 \tag{19}$$

where A is the electrochemically active surface area per unit volume, $j_{0,ref}^{H_2}$ is the reference exchange current densities. The hydrogen oxidation reaction order at hydrogen reference concentration ($CH_{2,ref}$) is γH_2. The charge transfer coefficient is α and its value is between 0 and 1, F is Faraday's constant and the activation over potential is $r)_{act}$. The subtitle "a" stand for anode side. The anode activation over potential $r)_a$ is determined as follows, respectively:

$$r)_a = \phi_e - \phi_i \tag{20}$$

$$r)_c = \phi_e - \phi_i - V_{oc} \tag{21}$$

where ϕ_e is electronic potential and ϕ_i is the ionic potential. V_{oc} is the open circuit voltage calculated by the Nernst's equation [5]:

$$V_{OC} = 1.317 - 2.769\times10^{-4}T + R_u T/2F \ln\left(p_{H2}\cdot p_{O2}^{1/2} \Big/ p_{H2O}\cdot p_{ref}^{1/2}\right) \tag{22}$$

where P_{ref} is the total pressure and F is Faraday's constant.

2.6 Thermal stress

In this study the detection of thermal stress is based on thermal strain. First the thermal strain, $\alpha(T-T_{ref})$, is calculated and then thermal stress, σ_{ii}, is determined by the strain, ε_{ii}, as defined by [28]:

$$\varepsilon_{xx} = \frac{1}{E}\left(\sigma_{xx} - \nu\sigma_{yy}\right) + \alpha\left(T - T_{ref}\right) \tag{23}$$

$$\varepsilon_{yy} = \frac{1}{E}\left(\sigma_{yy} - \nu\sigma_{xx}\right) + \alpha\left(T - T_{ref}\right) \tag{24}$$

$$\varepsilon_{xy} = \frac{1}{2G}\sigma_{xy} \tag{25}$$

where $\frac{1}{E}\left(\sigma_{xx} - \nu\sigma_{yy}\right)$ is the mechanical strain, α is the coefficient of thermal expansion, T is the temperature, T_{ref} is the strain reference temperature, E is the Young's ratio and ν is the Poisson's ratio. The shear modulus, G, is defined as:

$$G = \frac{E}{2(1+\nu)} \tag{26}$$

Rearranging Eqs. (23) and (24) the stress in x and y direction is determined as follows, respectively:

$$\sigma_{xx} = 2G\left[\varepsilon_{xx} + \frac{\nu}{1-2\nu}\left(-\frac{1+\nu}{\nu}\alpha\left(T - T_{ref}\right)\right)\right] \tag{27}$$

$$\sigma_{yy} = 2G\left[\varepsilon_{yy} + \frac{\nu}{1-2\nu}\left(-\frac{1+\nu}{\nu}\alpha\left(T - T_{ref}\right)\right)\right] \tag{28}$$

$$\sigma_{xy} = 2G\varepsilon_{xy} \tag{29}$$

2.7 Strain-displacement equation

Strain displacement equations, also called kinematic equations or Infinitesimal deformations, are as follows [29]:

$$\varepsilon_{xx} = \frac{\partial u}{\partial x} \tag{30}$$

$$\varepsilon_{yy} = \frac{\partial v}{\partial y} \tag{31}$$

$$2\varepsilon_{xy} = \frac{\partial u}{\partial x} + \frac{\partial v}{\partial x} \tag{32}$$

where u and v are the displacement which represents the unit charge in length of a line element.

2.8 Conservation of momentum for solid mechanics

The stresses can be indicated in terms of strains and displacements. The equation of motion in terms of stresses is [29]:

$$\sigma_{ij,j} + X_i = \rho \ddot{u}_i \tag{33}$$

where X_i is the body force which is negligible. $\ddot{u}_i$ is the acceleration of the particles inside the material and is zero ($\ddot{u}_i = 0$). So Eq. (34) will be:

$$\sigma_{ij,j} = 0 \tag{34}$$

Then

$$\frac{\partial \sigma_{xx}}{\partial x} + \frac{\partial \sigma_{xy}}{\partial y} = 0 \tag{35}$$

$$\frac{\partial \sigma_{yx}}{\partial x} + \frac{\partial \sigma_{yy}}{\partial y} = 0 \tag{36}$$

$$\sigma_{xy} = \sigma_{yx} \tag{37}$$

2.9 Energy equation

The energy equation for the porous electrodes is [29]:

$$K \nabla^2 T + \frac{Q}{K} + (3\lambda + 2\mu) T_0 \dot{\varepsilon} = \frac{1}{\alpha} \frac{\partial T}{\partial t} \tag{38}$$

where the coupling term between temperature and stress is $\dot{\varepsilon}$, the coefficient of linear thermal expansion is α and T_0 is the reference temperature.

3 BOUNDARY CONDITIONS

In order to model the crack initiation, the following expectations are utilized:

- The flow is laminar, steady and incompressible ($Ma < 0.3$).
- The reference temperature was equal to $800^{o}C$.
- Fuel is approximated as ideal gases, and gases mixture physical properties are estimated to ideal gas mixture law.
- Thermal diffusion is neglected.
- Neglected Stokes–Brinkman's assumption.
- Ohmic heat due to electron transfer is neglected because electronic conductivity in anode electrode is higher than ionic conductivity.
- All gasses behave as ideal gases.
- The Darcy equation is used to model mass transport in anode porous electrode.
- The coupling effect between the thermal and mechanical equations is neglected.

Based on the model provided in Fig.1 the following boundary conditions are applied.

3.1 Inlet boundary condition

At the anode electrode boundary.

$V = 0$

$U = U_{in}$

$T = T_0$

w_i = specified (mass fraction of the species).

No slip boundary condition is valid in all electrolyte boundaries due to U=0.

3.2 Outlet boundary condition

1- The conduction term compared to convection term can be neglected.
2- It is supposed that convection term is the dominant term in the mass transport model.

4 NUMERICAL PROCEDURE

A computational fluid dynamic (CFD) code based on a finite element method was developed and utilized. The code used a mapped rectangular meshes. The mapped rectangular consists of 725000 elements, 1285257 degree of freedom. The distribution of mesh numbers increases at the zones of (electrolyte –anode) the zone that the high temp and high pressure likely occurs. The mesh numbers decreased as it moves away from electrolyte to gas channel. The code obtains the temperature distribution in the following manner:

1) The code initially solves the secondary current distribution equation, Eqs. (17-22)
2) Then the code solves the non-linear momentum equations, Eqs. (7) and (8), for anode porous electrode and anode gas channel.
3) Furthermore, the code solves the species and the Stefan–Maxwell equations, Eqs. (9) through (14), for anode porous electrode.
4) Finally, the code solves the energy equation for porous cathode and anode and for solid electrolyte, Eqs. (15) and (16)

The obtained temperature distribution is used to solve the strain equations, Eqs. (23) through (29), to determine the thermal stress distribution. Then the code solves the strain displacement and energy equations, Eqs. (30) through (38), the thermal stress distribution, Its spread will be clear

5 RESULTS AND DISCUSSIONS

In order to confirm the results, we modified the current model and compared it to Roger's experimental data [25]. Fig. 2 reveals the comparison between the experimental and current study. We extracted our parameters of the present study from the Ghassemi [9], Hussain [26] and Shao [27, 28] studies (The rest of the validation input parameters were shown in Table 3). This comparison shown in Fig. 2 reveals a coherent result between the existing study and Roger's experiment with mean square error 1%.

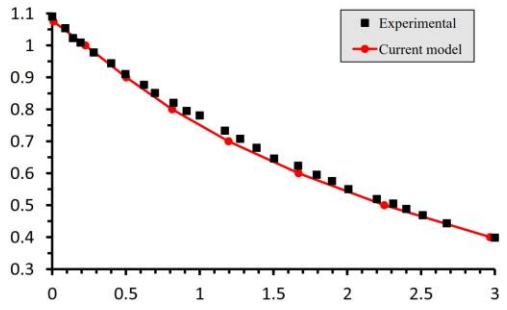

Fig.2
Present study data compared to Roger's experiment.

Table 3
Validation input parameter.

Description	Symbol	Value	unit
Operating temperature	T	800	^{0}c
Pressure	P_0	101335	P_a
Anode conductivity	σ	71428.57	S/m
Inlet velocity of fuel channel	$V_{in\ (fuel)}$	0.4	m/s
Reaction order of H_2 oxidation	γH_2	0.5	$A/m\text{-}^2$
Reference H_2 concentration	CH_2	10.78	Mol/m^3
Porosity of anode	ε	0.375	-
Tortuosity of anode	τ	4.5	-
Reference exchange current density for H_2	$J^{H_2}_{0,ref}$	1320	A/m^{-2}
Anode thermal conductivity	k_a	6.23	$W/m.K$
Specific heat of anode	$C_{p,a}$	595	$J/Kg.K$
Anode density	ρ_a	6870	Kg/m^3
Density of electrode	ρ_e	5900	Kg/m^3
Hydrogen dynamic viscosity	μH_2	$6.162 \times 10^{-6} + 1.145 \times 10^{-8} \times T$	
Water dynamic viscosity	μH_2O	$4.567 \times 10^{-6} + 2.209 \times 10^{-8} \times T$	$Pa.s$
Hydrogen thermal conductivity	kH_2	$0.08525 + 2.964 \times 10^{-4} \times T$	$W/m.K$
Water thermal conductivity	kH_2O	$-0.0143 + 9.782 \times 10^{-5} \times T$	$W/m.K$

6 PERFORMANCE ANALYSIS

Fig.3 shows the distribution of hydrogen molar concentration distribution at the center of anode electrode, through the *Y*-axis. As shown by the Fig 3., hydrogen fuel, H_2, molar concentration decreases as it nears the electrolyte. This phenomenon occurs due to consumption and production of electrons and ions at the electrode, see Eqs. (1) and (2).it is consumed and produce electrons and ions in these locations. The lowest concentration of fuel, H_2, obviously take place where the reaction is at the highest and that is at the border of the between the electrodes and the electrolyte
The porous electrolyte allows the transportation of gas species between anode and electrolyte. As H_2 flows in the fuel channels, they separate through the porous electrodes. After they diffuse, they react electrochemically where the electrochemical reactions take place, which is at the anode. This phenomenon is due to gas transfer from anode to electrolyte. H_2 will reach anode as H^{2+}. The migration of species and the hydrogen diffusive flux in the channel depend on all previously outlined.

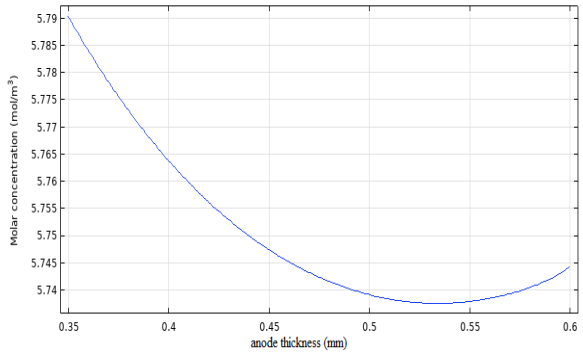

Fig.3
Molar concentration of H_2 at anode.

Fig. 4 depicts the pressure distribution at *Y*-axis across the middle of anode electrode. The pressure at the anode is about 5 *atm* and decreases when it gets near to electrolyte. At the middle of the anode the pressure is approximately zero. The electrochemical reaction increase as the pressure increases, the reactant concentration at the

response scenes increases. This in sequence improves the proportion of electrochemical reaction and the amount of mass transport in anode and cathode.

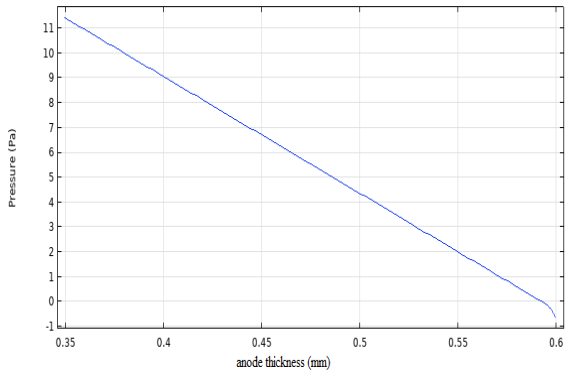

Fig.4
Pressure at Anode electrode.

The temperature shown in Fig. 5 is at the middle of anode electrode at $x = 30$. From this figure, the anode electrode approximately is acting at a temperature of about $1060^{o}C$ and the temperatures increases when it gets near to electrolyte.

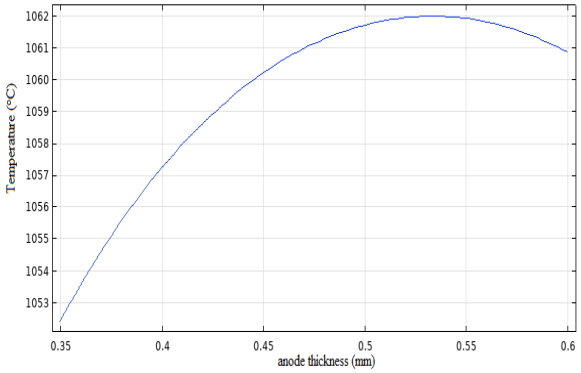

Fig.5
Temperature at anode electrode center.

Nearby to the fuel inlet close to anode electrode, excessive amount of heat is used by the endothermic reaction and causes a cold spot at this location. On the other hand, the temperature rises throughout the fuel channel due to exothermic electrochemical reactions, see Eqs. (4) and (5). As a result of the temperature increase, thermal stresses increases as well.

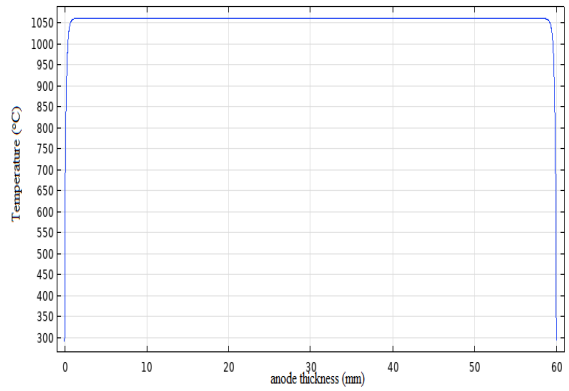

Fig.6
Temperature at Anode electrode near to electrolyte.

In Figs. (7,8) the distribution of temperature in the anode gas channel and anode are illustrated.

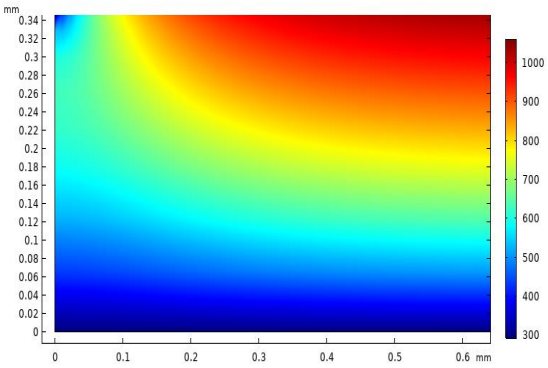

Left side (out let, x= 0.3)

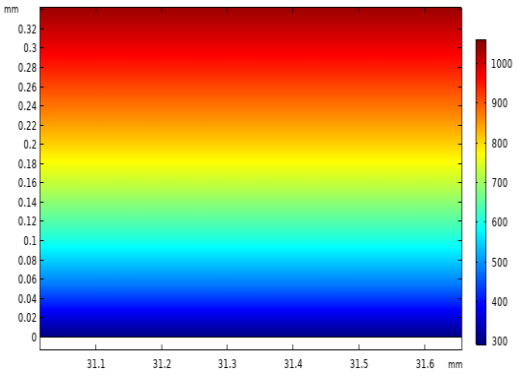

Middle (x=31)

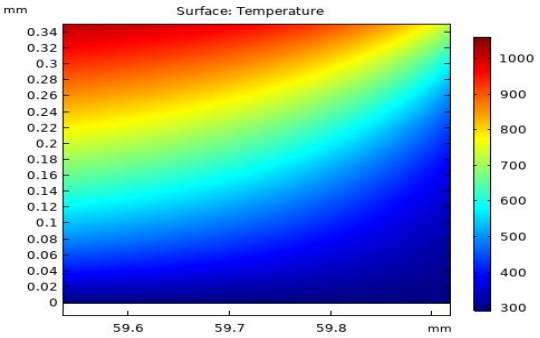

Right side (inlet, x= 59)

Fig.7
Temperature distribution at anode gas channel (^oC).

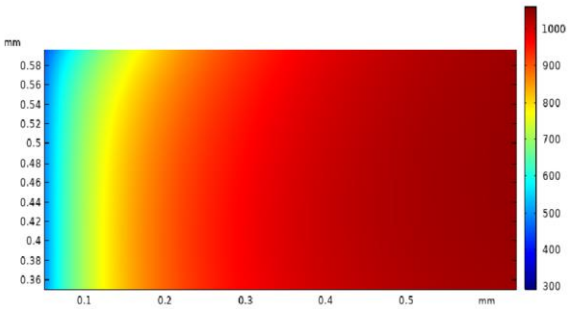

Left side (out let, x= 0.3)

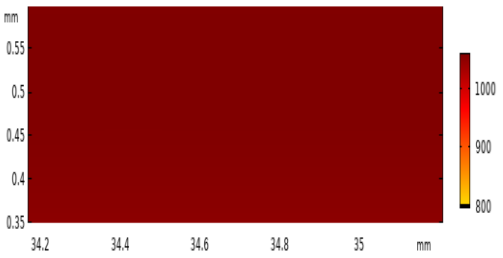

Middle (x=34)

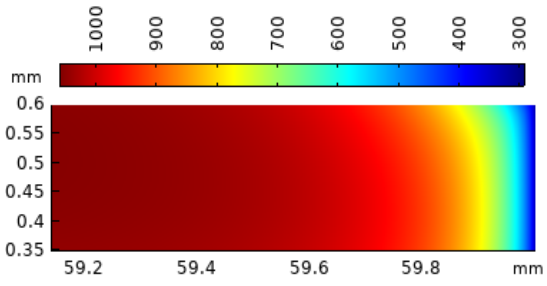

Right side (inlet, x= 59)

Fig.8
Temperature distribution at anode electrode.

As shown in Figs. 7 and 8, the distribution of temperature shows the follows:

- The temperature distribution is affected by the reforming and electrochemical reactions.

- In anode gas channel the temperature varied from $500^{o}C$ to $1100^{o}C$, the extreme temperature is in the middle near to the anode electrode and decreases as we go to inlet and outlet.
- In anode electrode, the maximum temperature is in the center and decreases as we go to right and left sides.
- There is a heat balance between endothermic with exothermic electrochemical reactions, and a higher temperature appears in active layer near electrolyte.
- The maximum temperature take place at the center of the anode electrode and decreases as it moves away from the center and goes to right and left sides.
- The exothermic electrochemical reactions cause the temperature to increase rapidly at the fuel inlet and outlet, the lower right corner and upper left corner of the channel, respectively.
- At the reaction site, the rate of electrochemical reaction is enhanced when the temperature increases.
- Since it is more difficult for H_2 gas to diffuse in the porous electrodes than in channels, the formed gradients of the H_2 molar concentration is larger in the fuel channel. Finally, higher temperatures increase the diffusivity of the species, conduct in minor values of concentration over-potentials.
- Local thermal stresses may be caused by high non-uniformity temperature distributions. The effects of mechanical characteristic gap can be examined by matching the stress distribution at each component's edge.

Fig. 9 depict the thermal stress distribution in anode electrode. The thermal stress is distributed in right and left part of anode electrode, while the maximum stress is in the right and left corners of lower parts, which is in contact with anode channel gas Fig. 8. Reduced performances can occur in case these stresses go beyond the threshold values dictated by the metal materials used for the construction of the SOFC. In addition to that, it can result in even a mechanical failure of the cell.

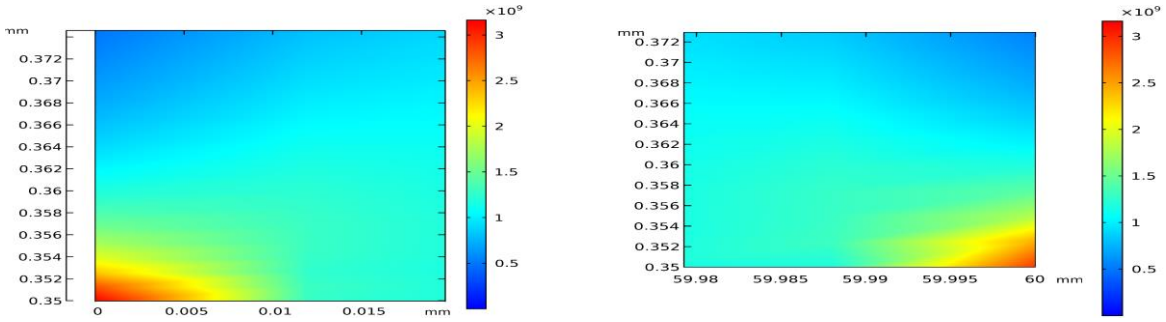

Left lower part

Right lower part

Fig.9
Thermal stress distribution at anode electrode.

From the above studies it had been noticed that there is a many factors that affect the thermal stress, one of these factors that had a basic effect is tortuosity. Tortuosity affected by temperature (high temperature), pressure, and porosity.

Figs. 10,11,12 shows the relation between tortuosity and the other factor. From Fig. 3 when tortuosity increase the temperature also increase. This is due to, when T increase, the forces between the atoms decreases, thus the tortuosites must increase.

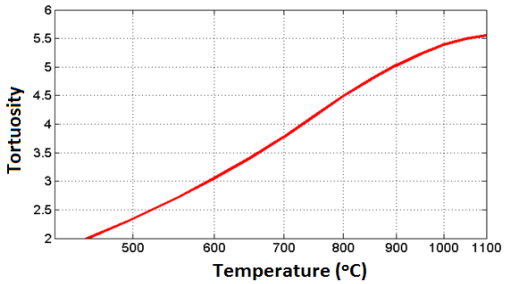

Fig.10
Relation between tortuosity and temperature.

After repeating the numerical code with different values of tortuosities in order to get the relation between tortuosity and pressure and how it varies. Fig. 11 depict that when tortuosity increase the pressure increase. This

phenomenon is due to, when the constant amount volume goes up, also temperature goes up, so the binding forces between atoms decrease, thus tortuosity increase.

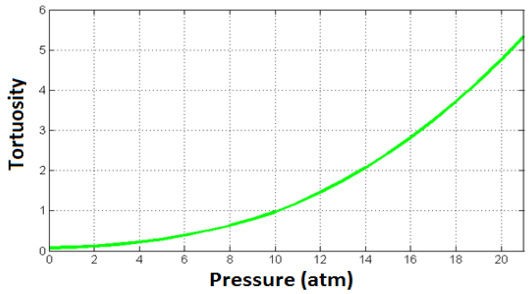

Fig.11
Relation between pressure and tortuosity.

Porosity is the measure of void space in material, also porosity has a direct relation with permeability. Porosity and permeability directly directed to tortuosity.

The relation between tortuosity and porosity is studied. From Fig. 12, it depicts that when tortuosity decrease, porosity increase. This phenomenon is due to, when porosity is high the void space is high which mean the tortuosity is low.

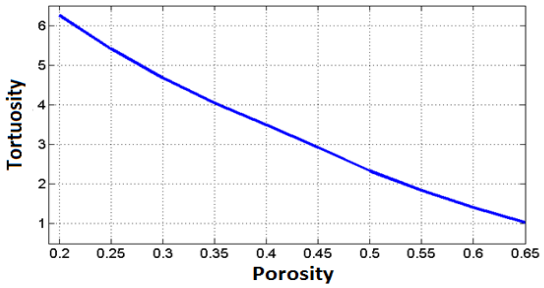

Fig.12
Relation between porosity and tortuosity.

A uniform temperature distribution is desirable for a SOFC, thermally induce stresses and strains which are undesirable as they can lead to cracking of the porous electrode, or mechanical failure. These are more liable to happen if the temperature gradient is large. In order to study the role of tortuosity and its efficiency on thermal stress, the study focus on the weakness zones like the edge boundaries of electrodes, so the study is at x=0 for anode and cathode electrodes. Fig. 13 shows that as tortuosity increases the thermal stress increase at the contact point between electrode and gas channel, which consider as a weak zone.

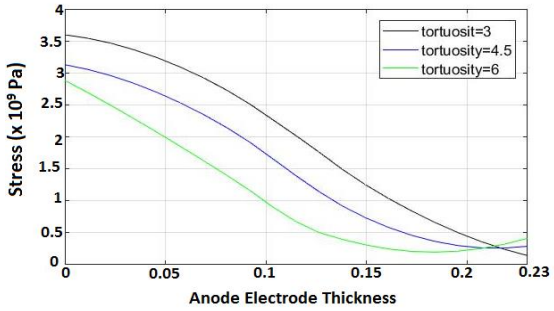

Fig.13
Stress at anode electrode.

7 CONCLUSION

In the current study thermal stress distribution as well as temperature distribution in the anode porous electrode is investigated. An in house code depended on finite element method is advanced and applied. The fuel is hydrogen, H_2, the operation temperature is between 800^oC to 1000^oC and the SOFC works at $0.8V$ continuously. The following

results are obtained. The stress in anode electrode affects the efficiency of the activation energy and the electrochemical reactions. It is based on matching the temperature, pressure, and thermal stress. The temperature distribution was concentrated at the middle of the contact area between anode and electrolyte up to the center of the anode electrode. Secondly, the pressure at the vertical bisector of anode was very high. And finally, the stress distribution was detected at the lower corners of the anode electrode with much more stress at the left corner than the right corner. Meanwhile, the life time of the anode electrode will be decreased because of the high thermal stress.

ACKNOWLEDGMENTS

The authors would like to thank Dr. Assil Fahs from American University of Beirut (AUB), and Dr. Mohammad Hassan Azan from JIA Engineering Group for their support and help.

REFERENCES

[1] Hoogers G., 2003, *Fuel Cell Technology Handbook*, CRC Press, Boca Raton.
[2] *Hibino T., 2002,* High Performance Anodes for SOFCs Operating in Methane-Air Mixture at Reduced Temperatures*, Journal of Electrochemistry Society* **149**: 133-136.
[3] Zhu H., 2005, Modeling elementary heterogeneous chemistry and electrochemistry in solid-oxide fuel cells, *Journal of Electrochemistry Society* **152**: 2427-2440.
[4] Greco F., 2014, Modelling the impact of creep on the probability of failure of a solid oxide fuel cell stack, *Journal of the European Ceramic Society* **34**: 2695-2704.
[5] Peksen M., 2015, Numerical thermomechanical modelling of solid oxide fuel cells, *Progress in Energy and Combustion Science* **48**:1-20.
[6] Boccaccini D.N., 2016, Investigation of the bonding strength and bonding mechanisms of SOFCs interconnector–electrode interfaces, *Material Letters* **162**: 250-253.
[7] Min X., 2016, Solid oxide fuel cell interconnect design optimization considering the thermal stresses, *Science Bulletin* **61**: 1333-1344.
[8] Fleischhauer F., 2015, Fracture toughness and strength distribution at room temperature of zirconia tapes used for electrolyte supported solid oxide fuel cells, *Journal of Power Sources* **275**: 217-226.
[9] Kamvar M., 2016, Effect of catalyst layer configuration on single chamber solid oxide fuel cell performance, *Applied Thermal Engineering* **100**: 98-104.
[10] Pianko-Oprych P., 2016, A numerical investigation of the thermal stresses of a planar solid oxide fuel cell, *Materials* **9**(10): 814.
[11] Pasaogullari U., Wang C.Y., 2003, Computational fluid dynamics modeling of solid oxide fuel cells, *The Electrochemical Society Proceedings* **7**: 1403-1412.
[12] Petruzzi L., 2003, A global thermo electrochemical model for SOFC systems design and engineering, *Journal of Power Sources* **118**: 96-107.
[13] Recknagle K.P., 2003, Three-dimensional thermo-fluid electrochemical modeling of planar SOFC stacks, *Journal of Power Sources* **113**: 109-114.
[14] Janardhanan V.M., Deutschmann O., 2006, CFD analysis of a solid oxide fuel cell with internal reforming: Coupled interactions of transport heterogeneous catalysis and electrochemical processes, *Journal of Power Sources* **162**: 1192-1202.
[15] Klein J.M., 2007, Modeling of a SOFC fuelled by methane: From direct internal reforming to gradual internal reforming, *Chemical Engineering Science* **62**: 1636-1649.
[16] Li P.W., Chyu M.K., 2003, Simulation of the chemical/electrochemical reactions and heat/mass transfer for a tubular SOFC in a stack, *Journal of Power Sources* **124**: 487-498.
[17] Suwanwarangkul R., 2006, Mechanistic modelling of a cathode-supported tubular solid oxide fuel cell, *Journal of Power Sources* **154**: 74-85.
[18] Celik S., 2015, Micro level two dimensional stress and thermal analysis anode/electrolyte interface of a solid oxide fuel cell, *International Journal of Hydrogen Energy* **40**: 7895-7902.
[19] Luo Y., Jiang W., 2016, Effects of anode porosity on thermal stress and failure probability of planar solid oxide fuel cell with bonded compliant seal, *International Journal of Hydrogen Energy* **41**: 7464-7474.
[20] Ho T.X., 2010, Effects of heat sources on the performance of a planar solid oxide fuel cell, *International Journal of Hydrogen Energy* **35**: 4276-4284.
[21] Bove R., Ubertini S., 2008, *Modeling Solid Oxide Fuel Cells, Methods*, *Procedures and Techniques, Fuel Cell and Hydrogen Energy*, Springer Publication.
[22] Singh P., Bansal P., 2008, *Advances in Solid Oxide Fuel Cells IV*, John Wiley Publications, New York.

[23] Ho T.X. 2010, Effects of heat sources on the performance of a planar solid oxide fuel cell, *International Journal of Hydrogen Energy* **35**: 4276-4284.
[24] Nehter P., 2008, *Theoretical Analysis of High Fuel Utilization Solid Oxide Fuel Cell*, Nova Science Publications, New York.
[25] Larminie J., Dicks A., 2003, *Fuel Cell Systems Explained*, John Wiley, New York.
[26] Akhtar N. 2009, A three dimensional numerical model of a single-chamber solid oxide fuel cell, *International Journal of Hydrogen Energy* **34**: 8645-8663.
[27] Milewski J., 2011, *Advanced Methods of Solid Oxide Fuel Cell Modeling*, Springer Publication.
[28] Boley B.A., Weiner J.H., 1997, *Fuel Theory of Thermal Stresses*, Dover Publication, New York.
[29] Hetnarski R.B., Eslami M.R., 2008, *Thermal Stress: Advanced in Theory*, Springer Publication.
[30] Rogers W. 2003, Validation and application of a CFD-Based model for solid oxide fuel cells and stacks, *International Conference on Fuel Cell Science Engineering and Technology* **2003**: 517-520.
[31] Hussain M.M. 2006, Mathematical modeling of planar solid oxide fuel cells, *Journal of Power Sources* **161**: 1012-1022.
[32] Shao Q., 2016, Influence of fluid flow and heat transfer on crack propagation in SOFC multi-layered like material with anisotropic porous layers, *International Journal of Solids and Structures* **97**: 189-198.
[33] Shao Q., 2015, An advanced numerical model for energy conversion and crack growth predictions in Solid Oxide Fuel Cell units , *International Journal of Hydrogen Energy* **40**: 16509-16520.